Eur. Phys. J. B **47**, 337–340 (2005)
DOI: 10.1140/epjb/e2005-00343-8

THE EUROPEAN PHYSICAL JOURNAL B

The role of material microstructure in the magnetic behavior of amorphous and polycrystalline Co_xSi_{1-x} lines

R. Morales, H. Rubio, M. Vélez[a], J.I. Martín, and J.M. Alameda

Departamento de Física, Facultad de Ciencias. Universidad de Oviedo, 33007 Oviedo, Spain

Received 12 May 2005
Published online 28 October 2005 –

Abstract. The role of material microstructure in the magnetic anisotropy of real nanostructures has been studied by the comparison of the magnetic behavior of arrays of amorphous and polycrystalline Co_xSi_{1-x}lines. From the experimental measurements of angular dependences of remanences parallel and perpendicular to the applied field we determine the angular dispersion of effective local easy axis of anisotropy. We have proved that amorphous lines have a dispersion of effective anisotropy axis much smaller than the polycrystalline samples. As a consequence, amorphous lines have a better defined magnetic behaviour, pointing the interest of the fabrication of nanostructures made of amorphous materials.

PACS. 75.75.+a Magnetic properties of nanostructures – 75.30.Gw Magnetic anisotropy – 75.50.Kj Amorphous and quasicrystalline magnetic materials

Co-Si compounds are currently used for applications such as low resistivity contacts in electronic devices [1,2] and, thus, magnetic nanostructures based in Co-Si alloys present a potential interest since they could be easily integrated in the existing silicon-based technology. A well defined magnetic behaviour is a prerequisite for these applications. And so the interplay between material microstructure and magnetic element geometrical dimensions, that plays a crucial role in determining the overall magnetic behaviour, must be determined. This issue is very relevant in samples made of polycrystalline material, particularly when geometrical dimensions become comparable to average grain size [3–6]. On the other hand, suggestions have been made that amorphous magnetic material, in which disorder occurs at a much smaller length scale, could provide a softer and more uniform magnetic behaviour [7,8].

In this work, we present the comparison of the magnetic behaviour of arrays of amorphous and polycrystalline submicron Co_xSi_{1-x} wires. This study is developed in order to analyze the competition between the lithographically defined shape anisotropy and the easy axis distribution induced by material microstructure. In this way, we try to determine which nanostructures are better to obtain a well defined magnetic behaviour, the amorphous ones or the polycrystalline ones. Structural transitions from polycrystalline to amorphous microstructure can be obtained in several ways such as by electron beam irradiation on a given sample or by changing the alloy composition. In this case, the simple binary Co_xSi_{1-x} system presents a well defined polycrystalline to amorphous transition for Co content below $x = 0.76$, which provides a good way to test the limitations in the fabrication process due to the scale of microstructural disorder: for $x < 0.76$ the films are amorphous with disorder occurring at the atomic length scale, whereas for $x > 0.76$ the films are polycrystalline with grain size only one order of magnitude below the width of the wires studied here [9].

In order to quantify the interplay in these materials between the two kinds of anisotropies (the coherent shape anisotropy due to patterning and the random anisotropy term originated by spatial fluctuations of the magnetocrystalline anisotropy axis due to material microstructure), we have developed a method that allows us to determine the angular dispersion of effective local easy axis of anisotropy (the easy axis of resultant anisotropy that acts over each magnetic moment) using only the experimental measurements of angular dependences of remanences parallel and perpendicular to the applied field.

Arrays of Co_xSi_{1-x} submicron wires have been prepared on Si substrates by electron beam lithography combined with a lift-off technique as reported elsewhere [10]. Two different arrays of lines of similar geometric dimensions have been used in this work: array A consists of $Co_{72}Si_{28}$ amorphous wires of thickness $t = 40$ nm, length $l = 250$ μm, and width $w = 280$ nm with interline separation 470 nm and array P consists of $Co_{81}Si_{19}$

[a] e-mail: mvelez@condmat.uniovi.es

polycrystalline wires, 40 nm thick, 250 μm long, 320 nm wide with interline separation 630 nm. In both cases interline distance is larger than wire width, ensuring that magnetostatic interactions between wires can be effectively neglected [11]. Typical grain size for the polycrystalline samples is about 15 nm, estimated from the width of the high angle X-ray diffraction peaks. The magnetic behavior of the arrays of lines in fields of up to 3 kOe has been characterized using a specifically designed Magnetooptical Transverse Kerr effect (MOTKE) setup [12]. This setup also allows to vary the angle ϕ_H between the applied field H and the lines direction. In it, a laser beam is focused on a 300 μm spot on the sample, so that the average magnetic response of the whole array of lines is obtained, and, by rotating the optical plane, both the magnetization components parallel ($M_{\rm p}$) and perpendicular ($M_{\rm t}$) to the applied field direction can be determined.

Thus, the hysteresis loops of the parallel and perpendicular magnetization components were obtained at each angle ϕ_H. From these hysteresis loops we have determined the polar plots of $M_{\rm p}(H)$ vs. $M_{\rm t}(H)$, which provide a good picture of the evolution of the average magnetization vector $\mathbf{m} = \mathbf{M}/M_{\rm s}$ as the field is decreased from saturation (see Fig. 1 for $\phi_H = 85°$). In both kinds of samples, $\mathbf{m}$ follows the circle of radius unity indicative of coherent rotation down to remanence and further beyond until the start of the switching process for negative magnetic field [12]. Figure 2 shows the angular dependence, from 0° to 90°, of the parallel and perpendicular components of the magnetization vector at remanence $m_{\rm p}(\phi_H) = M_{\rm p}(H = 0,\phi_H)/M_{\rm s}$ and $m_{\rm t}(\phi_H) = M_{\rm t}(H = 0,\phi_H)/M_{\rm s}$ for amorphous and polycrystalline arrays, compared with the predictions of the Stoner-Wolfarth model of coherent rotations under a simple uniaxial anisotropy term ($m_{\rm p}(\phi_H) = \cos\phi_H$ and $m_{\rm t}(\phi_H) = \sin\phi_H$). Actually, the magnitude of the magnetization vector at remanence $m(\phi_H) = [m_{\rm p}(\phi_H)^2 + m_{\rm t}(\phi_H)^2]^{1/2}$ is $1 \geq m(\phi_H) \geq 0.94$ for angles $0° \leq \phi_H \leq 88°$ in the two studied systems. Therefore, these two results (the prevalence of rotations down to remanence observed in the polar plots and the magnitude close to unity of the reduced magnetization remanence) rule out the presence of well defined magnetic domains at remanence, and suggests that there could be, at most, a magnetization ripple structure around the average magnetization direction that is responsible for the observed deviations from the simple Stoner-Wohlfarth behavior.

These results can be analyzed considering the studied lines as two dimensional random anisotropy ferromagnets since, due to their dimensions, the magnetization lies in the sample plane when the driving field is applied parallel to the substrate. Each magnetic moment is assumed to be subject to a local "magnetocrystalline" anisotropy that has the same strength $K_{\rm C}$ in every point of the system but the direction of the local easy axis fluctuates from one magnetic moment to another one. In general, $K_{\rm C}$ is not the true microscopic "magnetocrystalline" anisotropy $K^{\rm micro}$ acting on each magnetic atom but rather its average value $\langle K^{\rm micro}\rangle$ over a magnetic correlation length due to the coupling between the individual moments. That is, $K_{\rm C} = \langle K^{\rm micro}\rangle \approx K^{\rm micro}/N^{1/2}$, being $K^{\rm micro}$ the magnetocrystalline anisotropy of each individual grain or atom and N the number of grains within each correlated region [13]. The angular distribution of the local easy axis can be characterized by a certain normalized function $P(\phi_{\rm C})$, where $\phi_{\rm C}$ is the angle between the local easy axis and the lines direction, which is taken as the axis of reference for the angles appearing in this work. Due to the shape of the lines, there is a coherent anisotropy (of strength K_0) superposed to the random local "magnetocrystalline" anisotropy. The competitive effects of the shape anisotropy, the random magnetocrystalline anisotropy, and the exchange and magnetostatic interactions lead to a magnetization ripple structure at remanence [5,12]. This allows us to approximate the interactions between magnetic moments through a mean field $\lambda\mathbf{M}$, where λ is a phenomenological coupling parameter, and $\mathbf{M}$ the average magnetization. If the anisotropy field is $H_{\rm k} \equiv 2K_0/M_{\rm S}$, we can define the reduced magnitudes, $m \equiv M/M_{\rm S}$, and $\varepsilon \equiv \lambda M_{\rm S}/H_{\rm k}$, in terms of which the

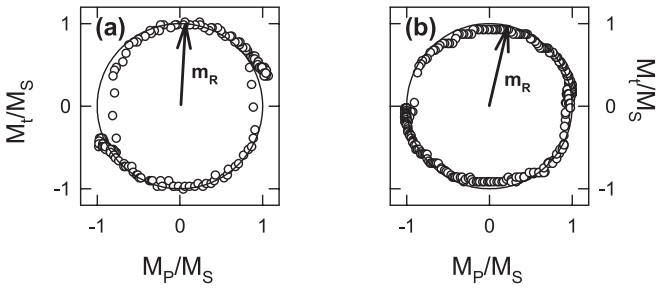

Fig. 1. Normalized polar plots of $M_{\rm p}(H)/M_{\rm s}$ vs. $M_{\rm t}(H)/M_{\rm s}$ at $\phi_H = 85°$ for: (a) amorphous lines; (b) polycrystalline lines. The position of magnetization at remanence is also indicated.

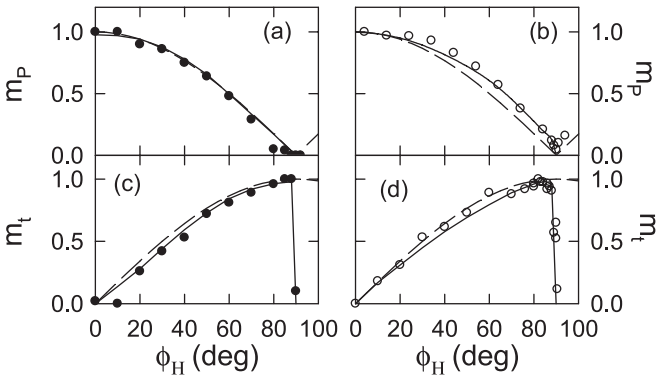

Fig. 2. Angular dependence of parallel and transverse remanences $m_{\rm p}(\phi_H) = M_{\rm p}(H = 0,\phi_H)/M_{\rm s}$ and $m_{\rm t}(\phi_H) = M_{\rm t}(H = 0,\phi_H)/M_{\rm s}$: (a) $m_{\rm p}(\phi_H)$ for amorphous arrays; (b) $m_p(\phi_H)$ for polycrystalline arrays; (c) $m_{\rm t}(\phi_H)$ for amorphous arrays; (d) $m_{\rm t}(\phi_H)$ for polycrystalline arrays. (•) and (o) are the experimental results. Dashed lines correspond to the $\cos(\phi_H)$ and $\sin(\phi_H)$ dependences expected for a Stoner-Wohlfarth model with uniaxial anisotropy. Solid lines are the theoretical fits obtained from equations (3) and (4) using the parameters indicated in the text.

reduced total energy density at remanence becomes

$$e = -\varepsilon m \cos(\phi - \phi_M) - \frac{1}{2}\delta_C \cos^2(\phi_C - \phi) - \frac{1}{2}\cos^2(\phi). \quad (1)$$

Here m is given by $m = \langle\cos(\phi\text{-}\phi_M)\rangle$, being ϕ the equilibrium position of the local magnetization, $\phi_{\rm M}$ the average magnetization direction, and $\delta_{\rm C} = K_{\rm C}/K_0$. Parallel and transverse remanences are $m_{\rm p}(\phi_H) = \langle\cos(\phi\text{–}\phi_H)\rangle$ and $m_{\rm t}(\phi_H) = \langle\sin(\phi\text{–}\phi_H)\rangle$ where the average values must be carried out over all easy axis directions satisfying $|\phi - \phi_{\rm M}| \leq \pi/2$ because we are considering the case of twofold local easy axis of anisotropy. From the condition for the stable equilibrium of magnetization at remanence and considering that ϕ, for any $\phi_{\rm C}$, is very close to $\phi_{\rm M}$ we find from equation (1) that

$$\phi \approx \phi_M + \frac{\delta_C}{2\varepsilon m}\sin\left[2(\phi_C - \phi_M)\right] - \frac{1}{2\varepsilon m_r}\sin(2\phi_M). \quad (2)$$

Taking into account equation (2), parallel and transverse remanences become

$$m_p(\phi_H) = \int_{\phi_M-(\pi/2)}^{\phi_M+(\pi/2)} \cos\left\{\phi_M - \phi_H + \frac{\delta_C}{2\varepsilon m} \times \sin\left[2(\phi_C - \phi_M)\right] - \frac{1}{2\varepsilon m}\sin(2\phi_M)\right\} P(\phi_C)\, d\phi_C \quad (3)$$

$$m_t(\phi_H) = \int_{\phi_M-(\pi/2)}^{\phi_M+(\pi/2)} \sin\left\{\phi_M - \phi_H + \frac{\delta_C}{2\varepsilon m} \times \sin\left[2(\phi_C - \phi_M)\right] - \frac{1}{2\varepsilon m}\sin(2\phi_M)\right\} P(\phi_C)\, d\phi_C. \quad (4)$$

We would like to emphasize that in equations (3) and (4), $m = m(\phi_H)$ and $\phi_{\rm M} = \phi_{\rm M}(\phi_H)$ can be obtained using only $m_{\rm p}(\phi_H)$ and $m_{\rm t}(\phi_H)$ measurements, because $m(\phi_{\rm H}) = [m_{\rm p}(\phi_{\rm H})^2 + m_{\rm t}(\phi_H)^2]^{1/2}$ and $\phi_M(\phi_H) = \phi_H + \arctan\left[m_t(\phi_H)/m_p(\phi_H)\right]$.

The experimental data points (ϕ_H, $m_{\rm p}(\phi_H)$) and (ϕ_H, $m_{\rm t}(\phi_H)$) of Figure 2 must be fitted to equations (3) and (4) which have three adjustable parameters: ε, δ_C and σ (where σ characterizes the disorder of distribution $P(\phi_C)$). The problem has been solved numerically using a non-linear least square algorithm [14] and assuming that $P(\phi_{\rm C})$ is a Gaussian distribution. The best numerical fit was obtained with the following parameters: $\varepsilon = 5$, $\delta_{\rm C} = 0.05$, and $\sigma = 40°$ for amorphous lines; $\varepsilon = 10$, $\delta_{\rm C} = 0.2$, and $\sigma = 30°$ for polycrystalline lines (see solid lines in Fig. 2). As it can be seen, a good agreement between experimental and theoretical results is found.

The angular distribution of anisotropy axis for the "magnetocrystalline" anisotropy term $P(\phi_{\rm C})$ obtained from the fit is shown in Figures 3a and 3b for the amorphous and polycrystalline lines respectively. For both

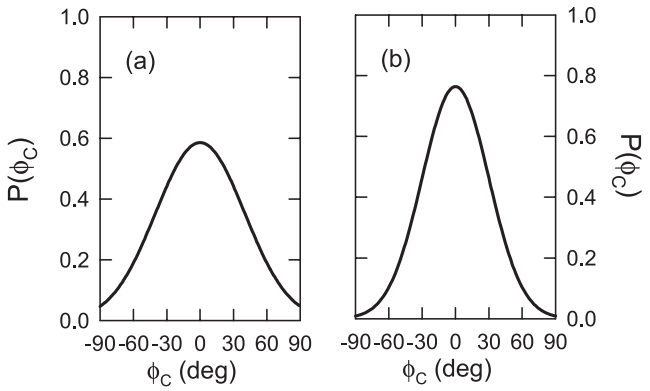

Fig. 3. Angular distribution of local anisotropy easy axes for the "magnetocrystalline" anisotropy term $P(\phi_C)$: (a) amorphous array; (b) polycrystalline array.

kinds of materials the "magnetocrystalline" local easy axes are distributed in a rather wide angular range (σ = 30°–40°) as expected from a random anisotropy model. The magnitude of the "magnetocrystalline" anisotropy $K_{\rm C}$ can be obtained from the deduced $\delta_{\rm C}$ values and the coherent shape anisotropy of the studied lines $K_0 = \frac{1}{2}(N_a - N_b)M_S^2$ (where $N_{\rm a} = 4\pi t/(w+t)$ and $N_{\rm b} = 0$ are the demagnetizing factors along the width and the length of the lines [15]). Taking into account the lines dimensions for each array, and that we have determined experimentally in reference continuous films $M_{\rm S}(Co_{72}Si_{28})$ = 320 emu/cm^3 and $M_{\rm S}(Co_{81}Si_{19})$ = 700 emu/cm^3, we obtain $K_0 = 8.0 \times 10^4$ erg/cm^3 and $K_0 = 3.4 \times 10^5$ erg/cm^3 for arrays A and P respectively. From this we find that $K_{\rm C} \approx 4.0 \times 10^3$ erg/cm^3 for amorphous lines and $K_{\rm C} \approx 6.8 \times 10^4$ erg/cm^3 for polycrystalline ones. It is interesting to stress that the combined effect of these anisotropies, K_0 and $K_{\rm C}$, of different physical origin is that an only effective uniaxial anisotropy K acts on each magnetic moment. Both the strength of this effective local anisotropy K and its direction $\phi_{\rm K}$ depend on the strength of K_0 and $K_{\rm C}$, and the angle $\phi_{\rm C}$ between the easy axis of the "magnetocrystalline" anisotropy and the line direction. Since we have already deduced $P(\phi_{\rm C})$ and the ratio $\delta_{\rm C} = K_{\rm C}/K_0$, and taking into account Crowther's calculations [16] about uniaxial anisotropies composition, the angular distribution of effective local easy axis $P(\phi_{\rm K})$ that act on each magnetic moment can be easily obtained and has been plotted in Figures 4a and 4b for the amorphous and polycrystalline lines respectively. In spite of the similar width in the angular distribution $P(\phi_{\rm C})$ for both materials, the microstructural disorder produces a much more important widening on the distribution function of effective local anisotropy axes $P(\phi_{\rm K})$ for the polycrystalline than for the amorphous lines (the half width is $\Delta\phi_{\rm K} = 6°$ for the polycrystalline array compared to $\Delta\phi_{\rm K} = 1.5°$ for the amorphous array). This difference is related with the magnitude of the local term $K_{\rm C}$ given by the numerical fit and highlights the convenience of working in materials with low anisotropy and small length scale for spatial fluctuations of the anisotropy axis, such as amorphous alloys, in order to obtain a well defined magnetic behaviour in nanostructures.

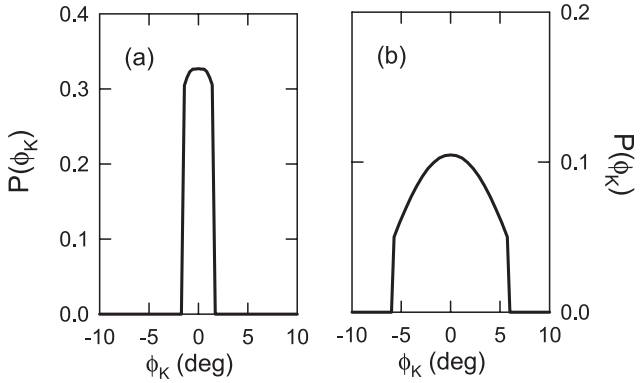

Fig. 4. Angular distribution of local effective anisotropy easy axes $P(\phi_{\mathrm{K}})$: (a) amorphous array; (b) polycrystalline array.

In summary, the role of microstructural disorder in the magnetic behavior and anisotropy of real nanostructures has been analyzed by the comparison of arrays of amorphous and polycrystalline Co_xSi_{1-x} lines. There are two different anisotropy contributions: the coherent shape anisotropy due to patterning and the random anisotropy term originated by spatial fluctuations of the magnetocrystalline anisotropy axis due to material microstructure. A unique anisotropy results from the joint effect of both anisotropies. Its angular dispersion has been determined from a mean-field approximation and from the angular dependence measurements of parallel and perpendicular remanences. We have proved that amorphous lines have an angular dispersion of effective anisotropy axis much smaller than the polycrystalline samples. As a consequence, amorphous lines have a better defined magnetic behaviour, pointing the interest of the fabrication of nanostructures made of amorphous materials.

Work supported by Spanish CICYT under grant MAT2002-04543-C02-01 and HF/2002-0170.

References

1. S.B. Herner, M. Mahajani, M. Konevecko, E. Kuang, S. Radigan, S.V. Dunton, Appl. Phys. Lett. **82**, 4163 (2003)
2. W.W. Wu, T.F. Chiang, S.L. Cheng, S.W. Lee, L.J. Chen, Y.H. Peng, H.H. Cheng, Appl. Phys. Lett. **81**, 820 (2002)
3. A. Fernandez, M.R. Gibbons, M.A. Wall, C.J. Cerjan, J. Magn. Magn. Mater. **190**, 71 (1998)
4. R. Morales, J.I. Martin, M. Velez, J.M. Alameda, F. Briones, J.L. Vicent, IEEE Trans. Magn. **38**, 2565 (2002)
5. T. Schrefl, J. Fidler, K.J. Kirk, J.N. Chapman, J. Appl. Phys. **85**, 6169 (1999)
6. J.I. Martín, J. Nogués, K. Liu, J.L. Vicent, I.K. Schuller, J. Magn. Magn. Mater. **256**, 449 (2003) and references therein
7. M. Velez, R. Morales, J.M. Alameda, F. Briones, J.I. Martin, J.L. Vicent, J. Appl. Phys. **87**, 5654 (2000)
8. M. Shima, M. Hwang, C.A. Ross, J. Appl. Phys. **93**, 3440 (2003)
9. M. Velez, C. Mény, S.M. Valvidares, J. Diaz, R. Morales, L.M. Alvarez-Prado, P. Panissod, J.M. Alameda, Eur. Phys. J. B **41**, 517 (2004)
10. J.I. Martin, M. Velez, R. Morales, J.M. Alameda, J.V. Anguita, F. Briones, J.L. Vicent, J. Magn. Magn. Mater. **249**, 156 (2002)
11. A.O. Adeyeye, J.A.C. Bland, C. Daboo, D.G. Hasko, Phys. Rev. B **56**, 3265 (1997)
12. R. Morales, J.I. Martin, M. Velez, J.M. Alameda, Eur. Phys. J. B **40**, 463 (2004)
13. R. Alben, J.J. Becker, M.C. Chi, J. Appl. Phys. **49**, 1653 (1978)
14. W.H. Press, S.A. Teukolsky, W.T. Vetterling, B.P. Flannery, *Numerical Recipes in FORTRAN*, 2nd edn. (Cambridge University Press, New York, 1992), Chap. 15
15. J.A. Osborn, Phys. Rev. **67**, 351 (1945)
16. T.S. Crowther, J. Appl. Phys. **34**, 580 (1963)